



Crystal Structure Prediction and Charge Density Distribution of Highly Energetic Dimethylnitraminotetrazole: a First Step for the Design of High Energy Density Materials

Arputharaj DAVID STEPHEN¹,
Ponnusamy SRINIVASAN¹, S.N. ASTHANA²,
Rajesh B. PAWAR² and Poomani KUMARADHAS^{1,*}

¹*Department of Physics, Periyar University, Salem 636 011, India*

²*High Energy Materials Research Laboratory,*

DRDO, Sutarwadi, Pune 411 021, India

**E-mail: kumaradhas@yahoo.com*

Abstract: The crystal structure of dimethylnitraminotetrazole has been predicted, based on systematically searching for densely packed structures within common organic crystal coordination types, followed by lattice energy minimization. The predicted crystal structures almost match the reported crystal structure determined by X-ray diffraction analysis. To understand the effect of the initial molecular geometry on the crystal packing, the crystal structure simulation was carried out for molecules taken from different environments, such as the X-ray structure (crystal field) and also from *ab initio* calculations (gas phase). The predicted crystal structures from both environments are very similar to the reported X-ray structure with a maximum deviation of 4.5%. The crystal density predicted from both methods is close to that reported. The bond topological, energetic and electrostatic properties of the isolated molecule from the predicted crystal structure have been determined using Bader's theory of atoms in molecules. The bond topological characterization reveals that the C–N bond is the weakest bond in the molecule. A large electronegative potential is found in the vicinity of the NO₂ group and the nitrogen-rich region of the tetrazole ring; these are probably the reactive sites of this molecule.

Keywords: energetic materials, crystal structure prediction, charge density analysis, atoms in molecules, electrostatic potential

Introduction

Crystal structure prediction emerged as a problem of outstanding importance in material science, both for the design of new materials and for understanding the behavior of polymorphic materials. In recent years, a large number of crystal structures of polymorphic forms and of some energetic molecules have been predicted [1-6]. The main advantages of predicting the crystal structure of highly energetic materials are: firstly, it gives the exact density of the energetic materials which is not possible to determine accurately by other methods, it largely simplifies the search for high density, energetic materials through trial synthesis of a large number of compounds and the design of potential explosive/propellant molecules of the same kind for civil and military applications. As far as highly energetic molecules are concerned, the trial procedure of synthesizing numerous energetic compounds is not a straightforward procedure, as it is hazardous and risk prone. Computational material design via molecular modelling, and both crystal structure prediction and charge density analysis are viable routes prior to the synthesis of highly energetic materials. The density of the material can be predicted from the crystal structure prediction procedure. There have been many successes [7] in predicting crystal structures, including the blind test [8] for searching for the global minimum lattice energy. Crystal structure prediction gives a large number of low-energy structures. The question is, which of these structures is the potentially stable, low-energy one. Since the energetic nature of explosives is mainly influenced by their density (packing of the molecules), material with high density would therefore be the primary objective for designing a highly energetic material. In order to estimate the crystal densities, the volume additivity approach [9-11] has been adopted in past decades. This combines the molecular volume with the molecular mass to obtain the density. Since this approach fails to merge the effects from the molecular conformations, Ammon and co-workers [12] developed a new procedure, and using that one can predict the crystal structure, the crystal density and molecular orientational effects. This procedure has been used successfully to perform crystal structure predictions for complex polycyclic hydrocarbons [10], polycyclic oxiranes [11] and several other molecules. Here we report the crystal structure prediction of the nitrogen rich, highly energetic 1,6-dimethyl-5-nitraminotetrazole molecule [13] (Figure 1).

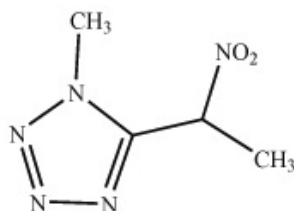


Figure 1. 1,6-dimethyl-5-nitraminetetrazole.

The combination of the tetrazole ring with energetic groups containing nitro groups [14], nitrate esters [15] or nitramines [16] is one of the current interests in explosive material research. Energetic materials based on tetrazoles show the desirable properties of high nitrogen content on one hand and astonishing kinetic and thermal stability due to aromaticity on the other hand. Compounds with high nitrogen content are potential candidates for replacing common secondary explosives like RDX [17], HMX [18] or high-tech propellants when combined with a suitable oxidizer [19]. Nitraminetetrazoles are of special interest, because these molecules exhibit oxidizer characteristics and possess the energetic, nitrogen-rich backbone that is rarely found in other energetic molecules [20]. Nitraminetetrazole is a modifier for the combustion rate of rocket propellants, cool gas generators and a special explosive in its own right [20]. To understand the energetic and explosive nature of a material, fundamental properties such as crystal density and a knowledge of the charge density distribution of the molecule are essential. In the present study, the crystal structure of the title compound has been predicted, and from that the crystal density was determined. These results were then compared with its reported crystal structure determined by X-ray diffraction [13]. Furthermore, the bond topological properties, such as electron density $\rho(r)$, the Laplacian of electron density $\nabla^2\rho(r)$, the energy density distribution and the electrostatic potential were calculated using the theory of Atoms in Molecules (AIM) [21]. This charge density study using quantum chemical calculations enables the bonds of the molecules to be characterized, which then allows the weak and the strong bonds in the molecule to be identified.

Computational details

Initially, the minimum energy geometry of the molecule was determined from the density functional theory [22, 23], B3LYP/6-31G* using the Gaussian03 package [24]. This optimized molecular geometry was then used as the initial geometry from which to generate the possible crystal structures of the molecule using MOLPAK (MOLEcular PAcKing) software [12]. After generating the initial crystal structures, lattice energy minimization was performed using the UMD

potential [25] in the PMIN package (latest version of WMIN) [26] to obtain the packing energy minimum hypersurface. The highest density and the lowest energy structure were selected as the best candidate. Thus, the predicted crystal structure (hereafter called IDEAL crystal structure) reproduced the reported X-ray crystal structure [13]. Alternatively, a similar crystal structure was also predicted from the molecular geometry of the reported experimental X-ray crystal structure (hereafter called EXPTL crystal structure). The unit cell parameters of both models of the predicted crystal structures (IDEAL and EXPTL) almost match the experimental structure, the difference being less than 4.5%. These promising unit cell values, predicted from the computational approach, are very encouraging and were further used to generate a crystal structure which is much closer to the experimental one.

To compute the bond topological (electron density, Laplacian of electron density, eigen values, and bond ellipticity) and the electrostatic properties (electrostatic potential, dipole moment and atomic charges) of the molecule, a single point energy DFT calculation was performed for the molecule removed from the crystal. The above mentioned charge density parameters were calculated from Bader's theory of atoms in molecules (AIM), which is implemented in the AIMPAC software [27]. The integrated charges were determined using the AIMALL software [28]. The deformation density and the Laplacian of the electron density of the molecule were plotted using wfn2plots and XD software packages [29]. The positive and negative electrostatic potential regions were visualized through the MOLISO package [30].

Results and Discussion

Crystal structure prediction

The crystal structure modelling was performed using a novel, intermolecular potential scheme, which has been used successfully for several C/H/N/O organic molecules [31, 32] in the recent years. The MOLPAK program was used to find the cell volume for each coordination type at 10° increments in the variable Eulerian rotational angles of the central molecule (search probe), thus considering 19³ hypothetical structures for each Eulerian angle, which varies between -90° and +90° to cover all unique orientations. The 25 most densely packed structures were refined to within 2° in the rotations and these structures were considered as hypothetical structures. In this way, MOLPAK considered 20 molecular coordination geometries, covering the space groups P1, P-1, P2₁, P2₁/c, C2/c, P2₁2₁2₁, Pca2₁, Pna2₁ and Pbca. Most of the space groups exist in more than one molecular coordination type. Each coordination exhibits different symmetry

relationships along the different axes for the 14 molecules in the coordination sphere, as established from the analysis of common coordination environments of organic molecules in the Cambridge Structural Database (CSD) [33]. The choice of the trial structures was constrained accordingly, so that the crystal structures had one molecule per asymmetric unit. This procedure generated 25 close packed, hypothetical structures in each of the 20 molecular coordination geometries, which provided 500 (20×25) possible starting points for the lattice energy minimization. Over 300 of these initial structures were energy minimized using PMIN with UMD potential. The program PMIN, which initially performed a Rosenbrock step refinement [34], followed by a least-squares refinement and lattice energy minimization by optimizing the cell constants, and translation and rotation of each rigid molecule in the unit cell to remove the cell strains, forces and torques.

As mentioned earlier in the computational section, there were two types of crystal structure models (EXPTL and IDEAL) which have been constructed for the chosen molecule. The EXPTL crystal structure denotes the crystal structure model constructed from the experimental X-ray molecular structure and corrected for the inadequacies of the X-ray structure determination by positioning the hydrogen atoms at a standard bond length for N=O at 1.22 Å and C–H at 1.098 Å along the bond directions [35]. The IDEAL crystal structure denotes the crystal structure model constructed from the optimized molecular structure. Thus the two constructed crystal structure models are well matched with the reported X-ray crystal structure geometry (Table 1).

Table 1. Unit cell parameters and the lattice energy of reported (XRAY) and the predicted (IDEAL & EXPTL) crystal structures

	XRAY [13]	IDEAL	EXPTL
Space group	Pbca	Pbca	Pbca
a (Å)	5.9555 (4)	5.7745(3)*	5.9067(0.8)*
b (Å)	13.2837(10)	13.8780(4.5)	13.5357(1.9)
c (Å)	17.4438(15)	17.4402(0)	17.6752(1.3)
$\alpha = \beta = \gamma$ (°)	90.0	90.0(0)	90.0(0)
V (Å ³)	1397.95	1397.63(0)	1413.2(1)
D _{cal} (gm/cm ³)	1.5222	1.5028(1.2)	1.4864(2.3)
E _{latt} (Kcal/mol)	-	20.05	-20.87

*Deviation in % from reported X-ray structure (XRAY).

Figure 2 displays the optimized geometry of the molecule and the superimposed form of the molecules lifted from the EXPTL, IDEAL and the XRAY crystal structures, respectively. The bond lengths, bond angles, and

torsion angles of the reported experimental (XRAY) [13], and the predicted molecular structures (IDEAL and EXPTL) are listed in Table S1. The predicted EXPTL structure almost matches the XRAY geometry, therefore, we made here a comparison only with the IDEAL structure. However, geometrically, the IDEAL structure shows some differences when compared with the XRAY and EXPTL structures; the exact differences can be found in Table S1. The N–N bond lengths of the tetrazole ring of the IDEAL structure range from 1.297 to 1.355 Å; these distances are very close to those reported for the XRAY structure. The nitramine (N–NO₂) bond is slightly longer (1.418 Å), and this trend remains the same in the C–N bonds of the molecule (see Table S1). The bond angles are also very similar to those reported for the XRAY [13] structure, with a maximum 2° difference for non-hydrogen bonded atoms; the angles are found to be slightly higher in C–H linked bonds [at atoms C(2) and C(3)]. Conformationally, in the IDEAL structure, the nitro and methyl groups attached to the C(1)–N(5) bond, were the most twisted compared with all other bonds in the molecule. This can be well understood from its torsion angles [C(3)–N(5)–C(1)–N(4): -29.4°, C(3)–N(5)–C(1)–N(1): 143.5°, N(6)–N(5)–C(1)–N(4): 114.4° and N(6)–N(5)–C(1)–N(1): 72.6°]; this large angular variation indicates that the NO₂ and CH₃ groups are rotated. But this effect is not present in the other methyl group attached bonds C(1)–N(1) or N(1)–N(2), which are rigid compared with the C(1)–N(5) bond.

Supplementary Table 1. Geometrical Parameters (Å, °)

Bonds	XRAY [13]	IDEAL	EXPTL
Bond lengths			
N(6)–O(1)	1.221	1.220	1.221
N(6)–O(2)	1.220	1.220	1.220
N(1)–N(2)	1.341	1.351	1.341
C(1)–N(1)	1.336	1.351	1.336
C(2)–N(1)	1.457	1.454	1.457
N(2)–N(3)	1.299	1.297	1.299
N(3)–N(4)	1.359	1.355	1.359
C(1)–N(4)	1.309	1.32	1.309
N(5)–N(6)	1.390	1.418	1.390
C(1)–N(5)	1.391	1.399	1.391
C(3)–N(5)	1.459	1.470	1.459
C(2)–H(1)	0.990	1.098	0.990
C(2)–H(2)	0.906	1.098	0.906
C(2)–H(3)	0.913	1.098	0.913
C(3)–H(4)	0.946	1.098	0.946
C(3)–H(5)	0.938	1.098	0.938
C(3)–H(6)	0.929	1.098	0.929

Bonds	XRAY [13]	IDEAL	EXPTL	Bonds	XRAY [13]	IDEAL	EXPTL
Bond Angles				Torsion Angles			
N(2)–N(1)–C(1)	107.3	107.3	107.3	C(1)–N(1)–N(2)–N(3)	0.7	1.6	0.7
N(2)–N(1)–C(2)	122.5	121.4	122.5	C(2)–N(1)–N(2)–N(3)	-177.4	180	-177.4
C(1)–N(1)–C(2)	130.2	131.3	130.2	N(2)–N(1)–C(1)–N(4)	-0.6	-1.4	-0.6
N(1)–N(2)–N(3)	106.9	106.9	106.9	N(2)–N(1)–C(1)–N(5)	-174.7	-175.4	-174.7
N(2)–N(3)–N(4)	110.7	111.1	110.7	C(2)–N(1)–C(1)–N(4)	177.3	-179.6	177.3
N(3)–N(4)–C(1)	104.9	105.5	104.9	C(2)–N(1)–C(1)–N(5)	3.2	6.5	3.2
N(6)–N(5)–C(1)	116.2	116.0	116.2	N(2)–N(1)–C(2)–H(1)	14.8	23.3	14.8
N(6)–N(5)–C(3)	118.0	115.3	118.0	N(2)–N(1)–C(2)–H(2)	-110.2	-97.3	-110.2
C(1)–N(5)–C(3)	120.6	118.7	120.6	N(2)–N(1)–C(2)–H(3)	121.8	142.5	121.8
O(1)–N(6)–O(2)	127.0	127.2	127.0	C(1)–N(1)–C(2)–H(1)	-162.8	-158.8	-162.8
O(1)–N(6)–N(5)	115.8	116.1	115.8	C(1)–N(1)–C(2)–H(2)	72.2	80.7	72.2
O(2)–N(6)–N(5)	117.2	116.6	117.2	C(1)–N(1)–C(2)–H(3)	-55.8	-39.5	-55.8
N(1)–C(1)–N(4)	110.2	109.2	110.2	N(1)–N(2)–N(3)–N(4)	-0.5	-1.2	-0.5
N(1)–C(1)–N(5)	123.7	125.3	123.7	N(2)–N(3)–N(4)–C(1)	0.1	0.3	0.1
N(4)–C(1)–N(5)	125.9	125.1	125.9	N(3)–N(4)–C(1)–N(1)	0.3	0.7	0.3
N(1)–C(2)–H(1)	106.6	107.4	106.6	N(3)–N(4)–C(1)–N(5)	174.2	174.7	174.2
N(1)–C(2)–H(2)	111.2	110.2	111.2	C(1)–N(5)–N(6)–O(1)	-168.8	-162.8	-168.8
N(1)–C(2)–H(3)	109.4	109.1	109.4	C(1)–N(5)–N(6)–O(2)	13.1	19.7	13.1
H(1)–C(2)–H(2)	114.2	110.6	114.2	C(3)–N(5)–N(6)–O(1)	-14.0	-17.5	-14.0
H(1)–C(2)–H(3)	99.8	110.1	99.8	C(3)–N(5)–N(6)–O(2)	167.8	164.9	167.8
H(2)–C(2)–H(3)	114.9	109.5	114.9	N(6)–N(5)–C(1)–N(1)	-78.5	-72.6	-78.5
N(5)–C(3)–H(4)	112.6	108.8	112.6	N(6)–N(5)–C(1)–N(4)	108.4	114.4	108.4
N(5)–C(3)–H(5)	110.3	111.6	110.3	C(3)–N(5)–C(1)–N(1)	127.4	143.5	127.4
N(5)–C(3)–H(6)	107.5	106.9	107.5	C(3)–N(5)–C(1)–N(4)	-45.7	-29.6	-45.7
H(4)–C(3)–H(5)	109.3	110.0	109.3	N(6)–N(5)–C(3)–H(4)	60.4	58.2	60.4
H(4)–C(3)–H(6)	108.8	110.1	108.8	N(6)–N(5)–C(3)–H(5)	-61.9	-63.3	-61.9
H(5)–C(3)–H(6)	108.4	109.5	108.4	N(6)–N(5)–C(3)–H(6)	-179.9	177.1	-179.9
				C(1)–N(5)–C(3)–H(4)	-146	-157.5	-146
				C(1)–N(5)–C(3)–H(5)	91.7	81.0	91.7
				C(1)–N(5)–C(3)–H(6)	-26.3	-38.6	-26.3

The unit cell parameters predicted from the two models are very close (Table 1) to the reported XRAY structure. Irrespective of the model, the tetrazole rings in the unit cell are arranged in two sections, as layers with an angle of intersection of 47.6° (XRAY), 41.3° (IDEAL) and 50.4° (EXPTL). The parallel distance between the first section of layers are: 7.07 \AA (along a-axis) and 2.82 \AA (along the b-axis), but these distances are different in the cases of the predicted IDEAL (5.592 ; 4.595 \AA) and the EXPTL (5.277 ; 4.548 \AA) structures. The differences are attributed to the slight differences in the cell parameters between the XRAY, IDEAL and

EXPTL structures. Invariably, the C(1)–N(1) bond overlaps in the tetrazole ring can be realized for all three model molecular structures. The shortened intermolecular contacts O(2)⋯O(2)ⁱ [$i=x+1/2, y, -z+1/2$] are noteworthy and their distances in the XRAY, IDEAL and EXPTL crystal structures are 3.350, 3.455 and 3.290 Å, respectively.

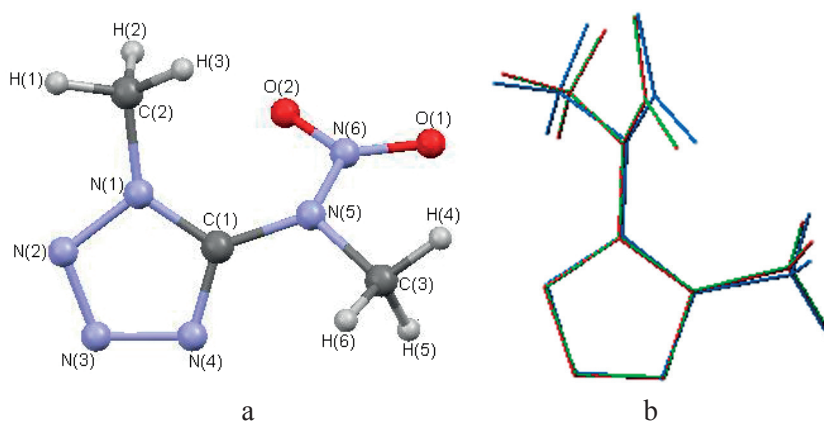


Figure 2. (a) Structure of the optimized molecule (gas phase) with atom labeling and (b) Superimposed form of molecules lifted from the XRAY (green), IDEAL (blue) and EXPTL (red) crystal structures, showing their conformational differences in the crystal.

Supplementary Table 2. Intermolecular hydrogen bonding interactions (Å, °)

H-bonds	(D⋯A)/D–H⋯A		
	XRAY [13]	IDEAL	EXPTL
C(2)–H(2)⋯O(1) ⁱ	3.191/125.1	3.412/139.0	3.205/122.2
C(2)–H(3)⋯N(2) ⁱⁱ	3.379/121.0	3.772/172.4	3.888/158.9
C(3)–H(6)⋯N(4) ⁱⁱ	3.586/147.4	3.517/138.5	3.593/147.4
C(3)–H(4)⋯N(4) ⁱⁱⁱ	3.460/144.0	3.505/131.8	3.443/139.6
C(3)–H(5)⋯O(1) ^{iv}	3.488/133.9	3.527/130.5	3.513/133.7
C(3)–H(5)⋯N(2) ^v	3.505/139.0	3.515/125.7	3.552/137.1

(i) $x-1/2, -y+1/2, -z$, (ii) $x+1/2, y, -z+1/2$, (iii) $x+1, y, z$, (iv) $-x+1, -y, -z$, (v) $-x+1/2, y-1/2, z$

The predicted structures (IDEAL and EXPTL) which packing pattern corresponds to the XRAY structure, is considered as a “correct” structure. Table 1 shows the differences of unit cells and the lattice energy between the predicted and the reported X-ray structure. When comparing the predicted unit cell with the experimental X-ray unit cell, the maximum deviation for the crystal structure

predicted (IDEAL) from the optimized molecular structure is 4.5%, and 1.9% for the crystal structure (EXPTL) predicted from the molecular structure of the reported X-ray structure [13]. Moreover, these crystal structures satisfactorily reproduce the intermolecular interaction distances (Table S2). From the list of the predicted IDEAL and EXPTL model structures, the correct crystal structure can be identified. For instance, in the IDEAL model, the correct structure present at the fifth position in the list and the energy difference between the correct structure and the structure in the first position in the prediction list (structure with lowest energy) is just 0.88 Kcal/mol and the corresponding difference in density is 0.013 g/cm³. Its unit cell parameters are: $a = 5.7745$, $b = 13.8780$, $c = 17.4402$ Å and the inter-axial angles are $\alpha = \beta = \gamma = 90^\circ$. Whereas, in the EXPTL model, the correct structure is present at the twelfth position in the predicted list; its corresponding unit cell parameters are: $a = 5.9067$, $b = 13.5357$, $c = 17.6752$ Å and the inter-axial angles are $\alpha = \beta = \gamma = 90^\circ$. These unit cell parameters do not deviate significantly (IDEAL: 4.5%; EXPTL: 1.3%) from the reported crystal structure [13]. However, the energy and density difference between the IDEAL and EXPTL predicted structures is 0.68 Kcal/mol and 0.04 g/cm³ respectively.

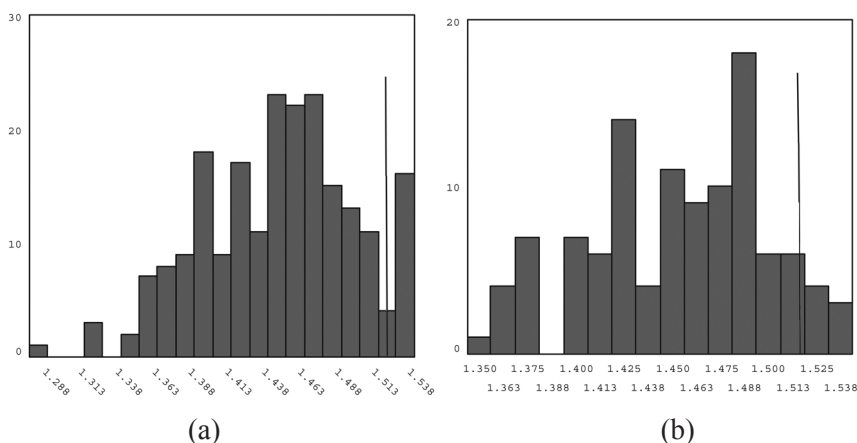


Figure 3. Histograms, showing the crystal density distribution of the (a) IDEAL and (b) EXPTL models. The bold line represents the reported experimental density (XRAY).

One of the most important properties of a highly energetic material is the explosive performance (detonation) [36, 37]. This largely depends on the density of the material. The histogram methodology has been used to understand the density distribution of the predicted structures (IDEAL and EXPTL), and their energy values lie within 1 Kcal/mol from the lowest predicted energy. This allows one to

validate the predicted density with the reported crystal density [13]. In the EXPTL model, several hundred structures fall within the 1 Kcal/mol energy range, whereas in IDEAL model only a few dozen structures fall within this range. Figure 3 shows histograms of density distribution for the predicted IDEAL and EXPTL crystal structures. The density distribution of the predicted crystal structures is found to be quite narrow ($0.1/0.2 \text{ g/cm}^3$) and the deviation of the predicted density from the experimental one is found to be small (0.02 to 0.2 g/cm^3).

Table 2. Bond topological properties of the molecule lifted from the XRAY (first line), EXPTL (second line) and IDEAL (third line) crystal structures

Bonds	$\rho_{\text{bcp}}(\text{r})^{\text{a}}$	$\nabla^2\rho_{\text{bcp}}(\text{r})^{\text{b}}$	λ_1^{b}	λ_2^{b}	λ_3^{b}	ϵ	d_1^{c}	d_2^{c}	D^{c}	$V(\text{r})$	$G(\text{r})$	$H(\text{r})$
N(1)–N(2)	2.57	-17.6	-21.4	-18.5	22.3	0.16	0.699	0.643	1.342	-4.13	1.45	-2.68
	2.56	-17.6	-21.4	-18.5	22.4	0.15	0.699	0.643	1.342	-4.13	1.45	-2.68
	2.51	-16.8	-20.8	-18	22.1	0.16	0.705	0.647	1.352	-4	1.41	-2.59
N(2)–N(3)	2.88	-22.7	-25.2	-21.3	23.7	0.18	0.663	0.64	1.303	-4.92	1.66	-3.26
	2.88	-22.7	-25.2	-21.3	23.7	0.18	0.663	0.64	1.303	-4.92	1.67	-3.26
	2.89	-22.9	-25.3	-21.4	23.8	0.18	0.662	0.64	1.301	-4.95	1.67	-3.27
N(3)–N(4)	2.49	-16.9	-20.1	-18.5	21.6	0.09	0.681	0.681	1.362	-3.89	1.35	-2.54
	2.49	-16.9	-20.1	-18.5	21.6	0.08	0.682	0.681	1.362	-3.89	1.35	-2.54
	2.51	-17.3	-20.3	-18.7	21.7	0.09	0.679	0.679	1.358	-3.94	1.37	-2.57
N(5)–N(6)	2.33	-14.8	-20.8	-16.1	22.2	0.29	0.677	0.713	1.39	-3.46	1.21	-2.25
	2.33	-14.8	-20.8	-16.2	22.2	0.29	0.678	0.712	1.391	-3.46	1.21	-2.25
	2.2	-13.0	-19.3	-15.2	21.5	0.27	0.691	0.727	1.418	-3.16	1.13	-2.03
C(1)–N(4)	2.57	-30.3	-22.0	-16.1	7.9	0.36	0.474	0.836	1.31	-6.54	2.21	-4.33
	2.57	-30.3	-22.0	-16.1	7.8	0.36	0.474	0.835	1.31	-6.54	2.21	-4.33
	2.52	-31.2	-21.3	-15.8	5.9	0.34	0.494	0.827	1.322	-5.94	1.88	-4.06
C(1)–N(1)	2.29	-18.2	-18.5	-13.8	14.1	0.34	0.457	0.88	1.337	-6.29	2.51	-3.78
	2.29	-18.2	-18.5	-13.8	14.1	0.34	0.456	0.88	1.336	-6.3	2.51	-3.79
	2.22	-20.0	-17.6	-13.3	10.8	0.33	0.47	0.883	1.352	-5.77	2.19	-3.59
C(1)–N(5)	2.07	-24.1	-15.9	-14.6	6.4	0.08	0.513	0.878	1.391	-4.33	1.33	-3
	2.07	-24.0	-15.8	-14.6	6.4	0.09	0.513	0.879	1.392	-4.32	1.32	-3
	2.05	-23.8	-15.8	-14.2	6.1	0.11	0.527	0.873	1.4	-4.03	1.18	-2.85
C(2)–N(1)	1.72	-15.2	-10.9	-10.8	6.4	0.01	0.517	0.94	1.457	-3.61	1.27	-2.34
	1.72	-15.2	-10.9	-10.8	6.4	0.01	0.517	0.94	1.457	-3.6	1.27	-2.34
	1.72	-15.1	-11.0	-10.7	6.7	0.02	0.513	0.941	1.454	-3.7	1.32	-2.38
C(3)–N(5)	1.71	-15.5	-11.0	-10.6	6.1	0.03	0.52	0.937	1.46	-3.48	1.2	-2.28
	1.71	-15.5	-11.0	-10.6	6.1	0.03	0.523	0.937	1.46	-3.49	1.2	-2.29
	1.68	-15.2	-10.7	-10.5	6	0.02	0.532	0.938	1.47	-3.3	1.12	-2.18
N(6)–O(1)	3.40	-23.0	-29.9	-27	33.9	0.11	0.592	0.628	1.221	-6.96	2.68	-4.29
	3.40	-23.1	-30.0	-27.1	33.9	0.11	0.592	0.628	1.22	-6.98	2.68	-4.3
	3.40	-23.0	-29.9	-27	33.8	0.11	0.591	0.629	1.22	-6.99	2.69	-4.3

N(6)–O(2)	3.40	-23.0	-29.9	-27.1	33.9	0.11	0.593	0.628	1.22	-6.96	2.67	-4.29
	3.40	-23.0	-29.9	-27.1	33.9	0.11	0.592	0.628	1.22	-6.96	2.68	-4.29
	3.40	-23.1	-29.9	-27	33.8	0.11	0.591	0.629	1.22	-6.97	2.68	-4.29
C(2)–H(1)	1.85	-22.9	-18.1	-17.5	12.6	0.03	0.714	0.365	1.079	-2.05	0.22	-1.83
	1.85	-23.0	-18.1	-17.5	12.6	0.03	0.714	0.365	1.079	-2.06	0.22	-1.83
	1.85	-23.1	-18.1	-17.6	12.6	0.03	0.714	0.365	1.079	-2.04	0.21	-1.83
C(2)–H(2)	1.85	-23.2	-18.2	-17.6	12.6	0.03	0.717	0.362	1.079	-2.03	0.2	-1.83
	1.85	-23.2	-18.2	-17.6	12.6	0.03	0.717	0.362	1.079	-2.03	0.2	-1.83
	1.86	-23.2	-18.2	-17.6	12.7	0.03	0.715	0.364	1.079	-2.05	0.21	-1.83
C(2)–H(3)	1.84	-22.4	-17.9	-17.1	12.6	0.04	0.709	0.371	1.08	-2.04	0.24	-1.81
	1.84	-22.4	-17.9	-17.1	12.6	0.04	0.709	0.371	1.08	-2.04	0.24	-1.81
	1.85	-22.7	-17.9	-17.3	12.6	0.03	0.709	0.37	1.08	-2.03	0.22	-1.81
C(3)–H(4)	1.85	-23.0	-18.1	-17.5	12.7	0.03	0.713	0.367	1.08	-2.04	0.22	-1.82
	1.85	-23.0	-18.1	-17.5	12.7	0.03	0.713	0.367	1.08	-2.04	0.22	-1.82
	1.86	-23.1	-18.2	-17.6	12.7	0.03	0.713	0.366	1.079	-2.05	0.22	-1.83
C(3)–H(5)	1.86	-22.9	-18.1	-17.5	12.7	0.03	0.711	0.368	1.08	-2.05	0.22	-1.83
	1.86	-22.9	-18.1	-17.5	12.7	0.03	0.711	0.368	1.08	-2.05	0.22	-1.83
	1.86	-22.9	-18.1	-17.5	12.7	0.03	0.712	0.368	1.08	-2.04	0.22	-1.82
C(3)–H(6)	1.85	-22.8	-18.0	-17.4	12.6	0.03	0.711	0.369	1.08	-2.04	0.22	-1.82
	1.85	-22.8	-18.0	-17.4	12.6	0.03	0.711	0.369	1.08	-2.04	0.22	-1.82
	1.85	-22.9	-18.0	-17.5	12.6	0.03	0.712	0.368	1.08	-2.04	0.22	-1.82

^a in eÅ⁻³, ^b in eÅ⁻⁵, ^c in Å.

Electron density distribution and the Laplacian of electron density

A (3,-1) type of bond critical points (bcp) [38] is found for all bonds of the molecule lifted from the crystal structures of the reported XRAY structure, and the predicted EXPTL and IDEAL crystal structures. The bond topological parameters of electron density at the critical points of each bond have been determined and are listed in Table 2. The electron density distribution pattern of the molecules lifted from the predicted structures (EXPTL and IDEAL) are in close agreement with the reported XRAY model [13]. Figure 4 shows the deformation density map of the molecules drawn from the IDEAL model. The electron densities $\rho_{\text{bcp}}(\mathbf{r})$ of the N–N bonds of the tetrazole ring are unequal. The charge accumulation found in the N(2)–N(3) bond [$\sim 2.88 \text{ eÅ}^{-3}$] is much higher than for the other two N–N bonds in the ring [N(1)–N(2): 2.55 , N(3)–N(4): 2.50 eÅ^{-3}]. For the nitramine (N–NO₂) the bond density [$\sim 2.33 \text{ eÅ}^{-3}$] is less, due to the effect of the NO₂ group on the bond. The bond density of C–N bonds with a methyl group attached is found to be equal with a value of $\sim 1.71 \text{ eÅ}^{-3}$. This density is very close to that reported for a similar structure [39], whilst the other C–N bond densities in the molecule are in the range ~ 2.05 to 2.57 eÅ^{-3} .

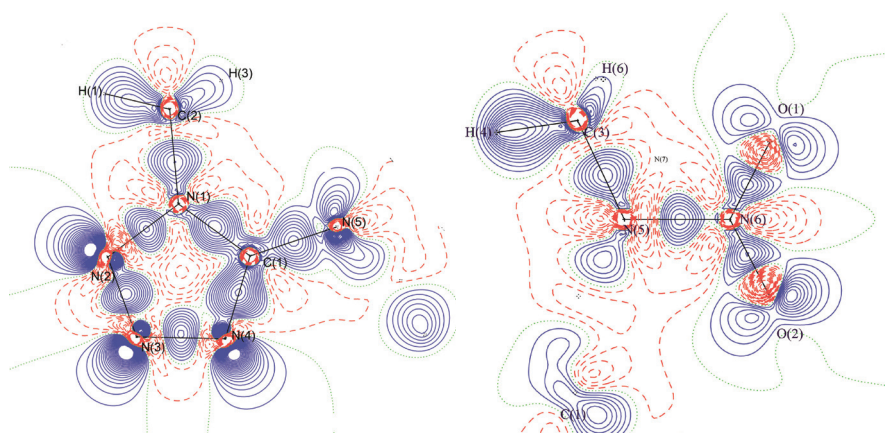


Figure 4. Deformation density map of the molecule shown in the plane of the tetrazole ring, and the nitro and methyl groups of the IDEAL structure. Contours are drawn at $0.05 \text{ e}\text{\AA}^{-3}$ intervals. Solid lines represent positive contours, dashed lines are negative contours and the dotted lines are zero contours.

Figure 5 displays the Laplacian of electron density $\nabla^2\rho_{\text{bcp}}(\mathbf{r})$ of the molecule in different planes, for the IDEAL model. The Laplacian of electron density for the N–N bonds of the tetrazole ring ranges from -16.8 to $-22.9 \text{ e}\text{\AA}^{-5}$, in which the N(1)–N(2) bond charges are more highly depleted than the other two bonds. Unlike the ring N–N bonds, the nitramine (N–NO₂) bond charges are highly depleted [$\sim -14.2 \text{ e}\text{\AA}^{-5}$]; this is attributed to the effect of the electron rich NO₂ group on the bonding electrons. This high charge depletion confirms that the N–NO₂ bond is the weakest bond in the molecule. The Laplacian of the C(1)–N(1) bond [$-18.8 \text{ e}\text{\AA}^{-5}$] is much less negative than the C(1)–N(4) bond [$\sim -30.6 \text{ e}\text{\AA}^{-5}$], indicating that the bond charges of the C(1)–N(4) bond are highly concentrated. But, the trend in the non-ring bond is different, where the C–N bonds with a methyl group attached [C(3)–N(5) and C(2)–N(1)] have charges which are not very concentrated, with values of $\sim -15.3 \text{ e}\text{\AA}^{-5}$; this large charge depletion confirms that these bonds are also weak.

The potential energy $V(\mathbf{r})$, kinetic energy $G(\mathbf{r})$ and the total energy density distribution of the molecule were also calculated to understand the energy density distribution of the molecule in the crystal. The total energy density distribution of N–N bonds of the ring [$\sim -2.60 \text{ H}\text{\AA}^{-3}$] are very similar except for the N(2)–N(3) bond [$\sim -3.27 \text{ H}\text{\AA}^{-3}$] (Table 2). The energy density of the ring C–N bond [$\sim -3.98 \text{ H}\text{\AA}^{-3}$] is higher than the other C–N bonds in the molecule.

The nitro group N–O [$\sim -4.29 \text{ H}\text{\AA}^{-3}$] and C(1)–N(4) bonds [$\sim -4.24 \text{ H}\text{\AA}^{-3}$] carry a high energy density in the molecule. The energy density distributions of other bonds are listed in Table 2.

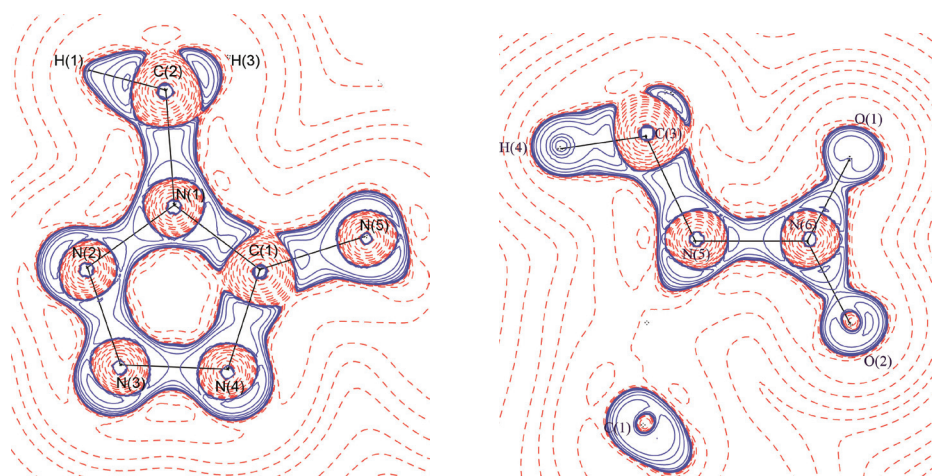


Figure 5. Laplacian of electron density of the molecule shown in the plane of the tetrazole ring and the nitro and methyl groups of the IDEAL structure. The contours are drawn at $2, 4$ and 8×10^n , $n = -2, -1, 0, 1, 2$. Solid lines show positive contours and negative contours are shown as dashed lines. The dotted lines are zero contours.

Electrostatic potential

The molecular electrostatic potential (MEP) explores the polarization, electron correlation, charge transfer effect and the reaction sites of the molecule [40-42]. Figure 6 shows the electrostatic potential of the molecule plotted for the isosurface values $+0.5$ and $-0.5 \text{ e}/\text{\AA}$. A large electronegative region is found near the nitrogen rich region [N(2), N(3) and N(4) atoms] of the tetrazole ring, being much higher than the electronegative region found in the vicinity of NO_2 group. These two regions are the expected nucleophilic sites of the molecule. The remaining areas are electropositive regions. The atomic charge distribution has been calculated from MPA [43], NPA [44] and AIM [45] models to understand the charge distribution in the molecule. The dipole moments of molecules lifted from the XRAY, EXPTL and IDEAL crystal structures have been determined. These are not equal and have values of 4.98, 4.85 and 4.16 Debye, respectively. The dipole moment of the molecule lifted from the IDEAL model is less than those for the other two structures.

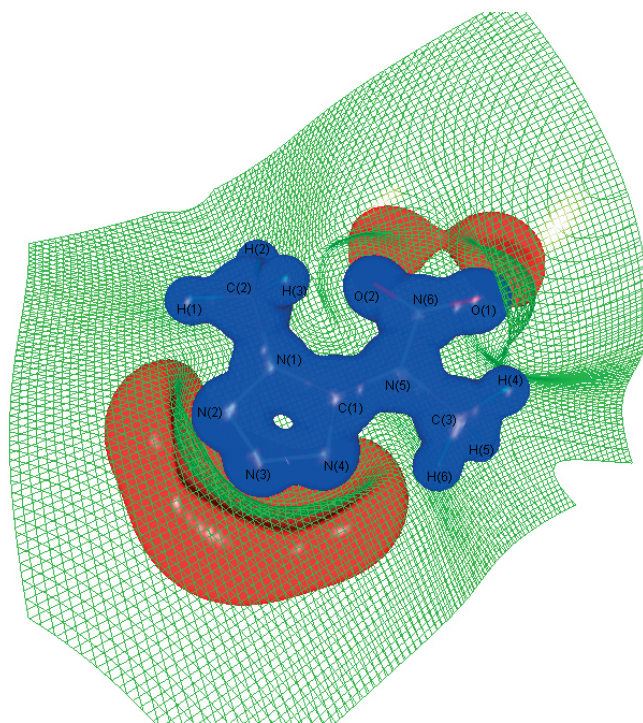


Figure 6. Isosurface representation of the electrostatic potential of the molecule lifted from the IDEAL structure. Blue: positive potential of ($0.5 \text{ e}\text{\AA}^{-1}$), red: negative potential ($-0.5 \text{ e}\text{\AA}^{-1}$) and green: zero potential.

Conclusion

The crystal structure of the energetic molecule dimethyl nitraminotetrazole has been successfully predicted. The predicted crystal structure from the optimized geometry (IDEAL), as well as the crystal structure predicted from the reported X-ray molecular structure (EXPTL) are in close agreement with the reported experimental unit cell, as well as the molecular geometric parameters. A maximum of 4.5% difference was found between the predicted and the reported unit cell structures in the unit cell parameters, which is a remarkable achievement for this study. Both models (IDEAL and EXPTL) reproduce the intermolecular interactions (hydrogen bonding) as reported in the X-ray crystal structure. The predicted hydrogen bond parameters are also found to be very close. These predicted parameters are very useful for modelling high density, energetic materials. Importantly, predicting the crystal structures through these

methods avoids synthesizing too many molecules (the trial and error method). To have a potential candidate (a material with high density) may limit the synthetic work which is probably hazardous in nature and a risk.

However, this method is not suitable for all molecular systems. The molecule lifted from the crystal structure has been used to understand the bond topological and the electrostatic properties of the molecule. The bond charges of the nitramine group (N–NO₂) are highly depleted, and it is the weakest bond in the molecule, whereas the N–N bonds in the tetrazole ring are found to be very strong. The C–N bonds with a methyl group attached are also weak, as found in TNT, but the BDE needs to be checked for comparison purposes. Large electronegative regions are found near the nitrogen rich area of the ring and in the vicinity of the NO₂ group, and these are the reactive locations of the molecule. The results from this study may help to model high density materials for the design of high energy density materials in the future.

Acknowledgements

The authors thank the DRDO-Armaments Research Board for financial support.

References

- [1] Price S.L., Computed Crystal Energy Landscapes for Understanding and Predicting Organic Crystal Structures and Polymorphism, *Acc. Chem. Res.*, **2009**, *42*, 117-126.
- [2] Hulme A.T., Price S.L., Tocher D.A., A New Polymorph of 5-Fluorouracil Found Following Computational Crystal Structure Predictions, *J. Am. Chem. Soc.*, **2005**, *127*, 1116-1117.
- [3] Vishweshwar P., McMahon J.A., Oliveira M., Peterson M.L., Zaworotko M.J., The Predictably Elusive Form II of Aspirin, *J. Am. Chem. Soc.*, **2005**, *127*, 16802-16805.
- [4] Sorescu D.C., Rice B.M., Thompson D.L., Intermolecular Potential for the Hexahydro-1,3,5-trinitro-1,3,5-s-triazine Crystal (RDX): A Crystal Packing, Monte Carlo, and Molecular Dynamics Study, *J. Phys. Chem. B*, **1997**, *101*, 798-808.
- [5] Block-Bolten A., Lee J., A Correlation Between the Chemical and Physical Properties of C, H, N, O Explosives, *J. Energ. Mater.*, **1988**, *6*, 107-128.
- [6] Rice B.M., Sorescu D.C., Assessing a Generalized CHNO Intermolecular Potential through *ab initio* Crystal Structure Prediction, *J. Phys. Chem. B*, **2004**, *108*, 17730-17739.
- [7] Bayer T., Lewis T., Price S.L., Which Organic Crystal Structures are Predictable by Lattice Energy Minimization?, *Cryst. Eng. Comm.*, **2001**, *44*, 178-212.
- [8] Lommerse J.P.M., Motherwell W.D.S., Ammon H.L., Dunitz J.D., Gavezzotti A., Hofmann D.W.M., Leusen F.J.J., Mooij W.T.M., Price S.L.,

- Schweizer B., Schmidt M.U., Van Eijck B.P., Verwer P., Williams D.E., A Test of Crystal Structure Prediction of Small Organic Molecules, *Acta Crystallogr. B*, **2000**, *56*, 697-714.
- [9] Cady H.H., Report LA-7760-M.S., Los Alamos Scientific Laboratory, N.M., *Chem. Abstr.*, **1980**, *92*, 149480-149505.
- [10] Marchand A.P., Zope A., Zaragoza F., Bott S.G., Ammon H.L., Du Z., Synthesis, Characterization and Crystal Density Modeling of Four C₂₄H₂₈ Cage-functionalized Alkenes, *Tetrahedron*, **1994**, *50*, 1687-1698.
- [11] Marchand A.P., Vidyand D., Liu Z., Kumar K.A., Zaragoza F., Talafuse L.K., Bott S.G., Watson W.H., Kashyap R.P., Ammon H.L., Synthesis, Characterization and Crystal Density Modeling of Polycarbocyclic Oxiranes, *Tetrahedron*, **1996**, *52*, 9703-9712.
- [12] Holden J.R., Du Z., Ammon H.L., Prediction of Possible Crystal Structures for C-, H-, N-, O-, and F-containing Organic Compounds, *J. Comp. Chem.*, **1993**, *14*, 422-437.
- [13] Karaghiosoff K., Klapötke T.M., Mayer P., Piotrowski H., Polborn K., Willer R.L., Weigand J.J., *N*-Nitroso- and *N*-Nitraminotetrazoles, *J. Org. Chem.*, **2006**, *71*, 1295-1305.
- [14] Adam D., Karaghiosoff K., Klapötke T.M., Holl G., Kaiser M., Triazidotrinetro Benzene: 1,3,5-(N₃)₃-2,4,6-(NO₂)₃C₆, *Propellants Explos. Pyrotech.*, **2002**, *27*, 7-11.
- [15] Karaghiosoff K., Klapötke T.M., Michailovski A., Nöth H., Suter M., Holl G., 1,4-Diformyl-2,3,5,6-Tetranitratopiperazine: A New Primary Explosive Based on Glyoxal, *Propellants Explos. Pyrotech.*, **2003**, *28*, 1-6.
- [16] Klapötke T.M., Chemistry of High-Energy Materials, Walter de Gruyter, Berlin, **2011**.
- [17] Deal W.E., Measurement of Chapman-Jouguet Pressure for Explosives, Temperature Dependence of Hammett Reaction Constants, *J. Chem. Phys.*, **1957**, *27*, 796-800.
- [18] Mader C.L., Report L.A.-2900, Los Alamos Scientific Laboratory, N.M., **1963**.
- [19] Urbański T., Chemistry and Technology of Explosives, Pergamon, England, **1985**.
- [20] Miller R.L., Technical Report, A.D.A., 182898, Morton Thiokol, Elkton, **1987**.
- [21] Bader R.F.W., Atoms in Molecules, *Acc. Chem. Res.*, **1985**, *18*, 9-15.
- [22] Perdew J.P., Density-functional Approximation for the Correlation Energy of the Inhomogeneous Electron Gas., *Phy. Rev. B*, **1986**, *33*, 8822-8824.
- [23] Becke A.D., Density-functional Thermochemistry. III. The Role of Exact Exchange, *J. Chem. Phys.*, **1993**, *98*, 5648-5652.
- [24] Frish A., Leen E., Nielson A.B., Holder A.J., Roy Dennigton R.D., Keith T.A., *Gaussian Incorporated*, Pittsburgh PA, **2005**.
- [25] Holden J., Du Z., Ammon H.L., Prasad S., Wells E., Albu N., Structure Predictions with MOLPAK, WMIN and PMIN, **2009**.
- [26] Busing W.R., WMIN – a Computer Program to Model Molecules and Crystals in Terms of Potential Energy Functions, Report ORNL-5747, Oak Ridge National Laboratory, Oak Ridge, **1981**.

- [27] Cheeseman J., Keith T.A., Bader R.F.W., AIMPAC Program Package McMaster University Hamilton, Ontario, **1992**.
- [28] Keith T.A., AIMAll **2009**, (Beta Version 09.08.26).
- [29] Koritsanszky T., Macchi P., Gatti C., Farrugia L.J., Mallinson P.R., Volkov A., Richter T., XD-2006. A Computer Program Package for Multipole Refinement and Topological Analysis of Charge Densities and Evaluation of Intermolecular Energies from Experimental or Theoretical Structure Factors, **2007**, Version 5.33.
- [30] Hubschle C.B., Luger P., *Mollso* - a Program for Colour-mapped Iso-surfaces, *J. Appl. Cryst.*, **2006**, *39*, 901-904.
- [31] Coombes D.S., Price S.L., Willock D.J., Lesile M., Role of Electrostatic Interactions in Determining the Crystal Structures of Polar Organic Molecules. A Distributed Multipole Study, *J. Phys. Chem.*, **1996**, *100*, 7352-7360.
- [32] Coombes D.S., Nagi G.K., Price S.L., On the Lack of Hydrogen Bonds in the Crystal Structure of Alloxan, *Chem. Phys. Lett.*, **1997**, *265*, 532-537.
- [33] Allen F.H., Kennard O., 3D Search and Research Using the Cambridge Structural Database, *Chem. Design Automation News*, **1993**, *8*, 31-37.
- [34] Savenco V., Hundsdorfer W., Verwer J.G., A Multirate Time Stepping Strategy for Stiff ODEs, *BIT Numer. Math.*, **2007**, *47*, 137-155.
- [35] Allen F.H., Kennard O., Watson D.G., Brammer L., Orpen A.G., Taylor R.J., Tables of Bond Lengths Determined by X-ray and Neutron Diffraction. Part 1. Bond Lengths in Organic Compounds, *Chem. Soc. Perkin Trans.*, **1987**, *2*, S1-S19.
- [36] Cooper P.W., *Explosive Engineering*, Wiley-VCH, New York, **1996**.
- [37] Olah G.A., Squire D.A., *Chemistry of Energetic Materials*, Academic Press, Inc. London, **1991**.
- [38] Popelier P.L., *Atoms in Molecules: An Introduction*, Prentice Hall, U.K., **2000**.
- [39] Stephen A.D., Pawar R.B., Kumaradhas P., Exploring the Bond Topological Properties and the Charge Depletion-impact Sensitivity Relationship of High Energetic TNT Molecule via Theoretical Charge, Density Analysis, *J. Mol. Struct. (THEOCHEM)*, **2010**, *959*, 55-61.
- [40] Su Z., Coppens P., On the Mapping of Electrostatic Properties from the Multipole Description of the Charge Density, *Acta Crystallogr. A.*, **1982**, *48*, 188-197.
- [41] *Molecular Electrostatic Potentials: Concepts and Application*, (Mishra P.C., Kumar A., Murray J.S., Sen K.D., Eds.), Elsevier, Amsterdam, **1996**.
- [42] Volkov A., Gatti C., Abramov Y., Coppens P., Evaluation of Net Atomic Charges and Atomic and Molecular Electrostatic Moments Through Topological Analysis of the Experimental Charge Density, *Acta Crystallogr. A*, **2000**, *56*, 252-258.
- [43] Mulliken R.S., Electronic Population Analysis on LACO-MO Molecular Wave Functions, *J. Chem. Phys.*, **1995**, *23*, 1833-1840.
- [44] Reed A.E., Weinstock R.B., Natural Population Analysis, *J. Chem. Phys.*, **1985**, *83*, 735-746.
- [45] Bader R.F.W., Nguyen-Dang T.T., Quantum Theory of Atoms in Molecules – Dalton Revisited, *Adv. Quantum Chem.*, **1981**, *14*, 63-124.

